Single-photon vortex beam detection with near-field diffraction

Sarayut Deachapunya[*]

Department of Physics, Faculty of Science, Burapha University, ChonBuri Province 20131, Thailand;
Quantum and Nano Optics Research Unit, Burapha University, ChonBuri Province 20131, Thailand;
and Thailand Center of Excellence in Physics, Ministry of Higher Education, Science, Research and Innovation,
328 Si Ayutthaya Road, Bangkok 10400, Thailand

Sorakrai Srisuphaphon, Sitti Buathong, and Pissunee Deechuen

Department of Physics, Faculty of Science, Burapha University, ChonBuri Province 20131, Thailand
and Quantum and Nano Optics Research Unit, Burapha University, ChonBuri Province 20131, Thailand

A beam of single-photon vortex has been detected with near-field diffraction. Our single-photon beam is generated with a weak coherent pulse method and subsequently imprinted with the orbital angular momentum of the vortex using a zeroth-order vortex half-wave retarder. The detection is employed with a two-grating Talbot near-field effect. Instead of using expensive single-photon image detection, we use a mask grating and an avalanche photodiode for the detection. This technique can identify the order and charge of the vortex from different count rates. Our technique can be utilized in the field of quantum information technology such as quantum cryptography using orthogonal states of an optical vortex beam.

I. INTRODUCTION

An optical vortex is a whirlpool of light in which its phase spirals around the optical beam axis. It is known to retain the orbital angular momentum (OAM) of $l\hbar$ and the topological charge of l per photon [1,2]. The discovery of this phase singularity has opened new areas in classical and quantum optics, owing to various potential applications [3,4]. Vortices of single photons have been at the center of interest in the active field of quantum optical computing and information [5,6]. These twisted photons are exploited as qubits or qudits formed by quantum states, which involve countless different OAM states that are orthogonal to each other, as well as superpositions of these OAM states. These states are independent of the light's spin angular momentum (SAM), corresponding to circular polarization states [7]. The use of OAM quantum states allows for improved channel capacity and noise immunity [8]. Various studies on the quantum nature of OAM single photons have been carried out. A simple configuration for OAM encoding of a single photon was utilized as a unitary operator in quantum computation [9]. Orbital angular momentum states of single photons can offer multidimensional quantum entanglements [5,10,11] and multiple high-dimensionally entangled photons [12–14]. Photon quantum states of the spin-orbit degree of freedom have been investigated for quantum entanglement using artificially engineered surfaces [15] and for quantum teleportation using linear optics [16]. Orbital angular momentum single photons and their SAM-OAM hybrid states also play roles in quantum cryptography based on OAM quantum key distribution, which has been scrutinized recently [17–19]. To employ OAM single photons in quantum applications, a detection system is required to efficiently distinguish single-photon vortices. Setups for identifying the OAM and SAM of an individual photon using a Mach-Zehnder interferometer and prisms have been proposed, based on their rotational phase symmetry [20]. Diffractive elements have also been used to characterize the OAM of single photons [21] and could be replaced by refractive components to improve the detection efficiency [22]. An electron-multiplying CCD camera with high gain has been used to image complex optical fields, such as vortex knots [23], and vortex arrays with a method of spiral phase filtering [24] at the single-photon level. Previously, the Talbot effect [25] was achieved with single photons [26] and demonstrated for OAM measurements of optical vortices [27–33]. The electromagnetic near fields, induced by plasmons generated by light at the single-photon level, have been shown to influence quantum interference and provide control over quantum-mechanical systems [34]. A conditional quantum detection of plasmonic near fields has also been recently proposed to manipulate quantum noise for sensing [35]. In this paper, sorting OAM single photons with the Talbot effect is performed using diffraction and mask gratings. The single-photon vortices are generated with a weak coherent pulse (WCP) technique and a vortex half-wave retarder (VHWR).

II. THEORY AND METHODS

In Fig. 1 the theoretical schematic illustrates the propagation of light with wavelength λ, and with an OAM state l, diffracting through the gratings G_1 and G_2 in the near-field
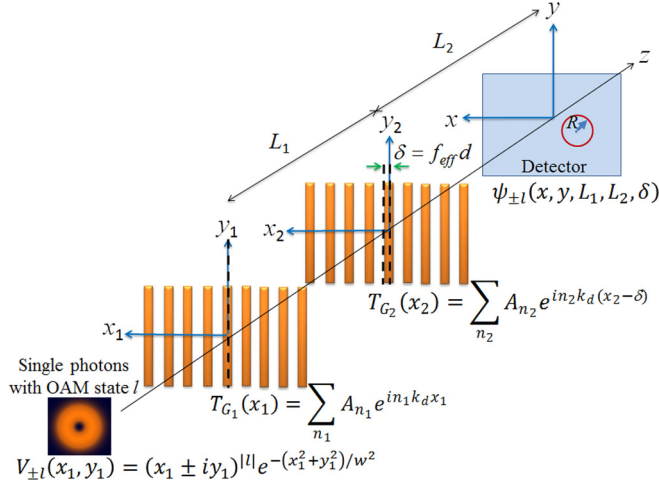
———————
[*]sarayut@buu.ac.th

FIG. 1. Theoretical diagram for propagation from left to right, where an incoming wave with OAM state l in the form of the wave function $V_{\pm l}$ diffracts through gratings G_1 and G_2. These gratings are represented by the transmission function $T_{G_{1,2}}$, with an overlap distance δ. The resulting Talbot interference patterns are observed on the screen at the xy plane.

regime. The gratings have an identical period of d and an open fraction of $f = 0.5$. When the distance L_1 equals the Talbot length $L_T = d^2/\lambda$, the system consisting of these two gratings can be regarded as a single grating with an effective open fraction $f_{\text{eff}} < 0.5$ provided the overlap distance δ is less than $d/2$. The distance δ is correlated to the effective open fraction f_{eff} by the relation $\delta = f_{\text{eff}} d$ [30]. Utilizing a small value of f_{eff}, it becomes possible to more clearly observe distinct OAM states via the Talbot effect [31]. On expressing the wave function of OAM states in Gaussian form $V_{\pm l}(x_1, y_1)$ and representing the transmission functions of the gratings as a Fourier series (Fig. 1), performing the Fresnel integrals enables us to obtain the exact wave function [30,31]

$$
\begin{aligned}
&\psi_{\pm l}(x, y, L_1, L_2, \delta) \\
&= C_l(L_1, L_2) \sum_{n_1, n_2} A_{n_1} A_{n_2} f_{n_1, n_2}^{|l|}(x, y, L_1, L_2) \exp\left[-\beta(L_1, L_2)\right. \\
&\quad \times \left|f_{n_1, n_2}(x, y, L_1, L_2)\right|^2 - i g_{n_1, n_2}(x, L_1, L_2, \delta)\right],
\end{aligned} \tag{1}
$$

where

$$
f_{n_1, n_2}(x, y, L_1, L_2) = \left(x + n_1 d \frac{L_1 + L_2}{L_T} + n_2 d \frac{L_2}{L_T}\right) \pm iy,
$$

$$
\beta(L_1, L_2) = \frac{k(2L_1 + ikw^2)}{2L_2[kw^2 - 2i(L_1 + L_2)]},
$$

$$
\begin{aligned}
g_{n_1, n_2}(x) &= n_1 k_d x \frac{L_1}{L_2} + n_2 k_d \delta \\
&\quad + \frac{n_1^2 \pi L_1}{L_T}\left(1 + \frac{L_1}{L_2}\right) + 2\pi n_1 n_2 \frac{L_1}{L_T}. \tag{2}
\end{aligned}
$$

Here the wave number $k = 2\pi/\lambda$. The multiplier $C_l(L_1, L_2)$ includes constants and variables independent of the xy coordinates on the detector. The Fourier coefficient $A_{n_j} = \sin(n_j \pi f)/n_j \pi$ for the transmission function of grating

$T_{G_j}(x_j)$ exhibits periodicity along the transverse axis with the period $k_d = 2\pi/d$ [36].

For a single-photon source, the collision rate of photons at specific xy coordinates on the detector screen corresponds to the distribution of intensity, or the squared modulus of the wave function, $|\psi_{\pm l}|^2$ [26]. Hence, the count rate of photons is affected by the OAM state l, as well as the distances δ, L_1, and L_2. Suppose there is a circular region on the screen that represents the photon detection area, which corresponds to the size of a photon detector. This circular region is indicated by the center (x_c, y_c) and has a radius of R in Fig. 1. The count rate, which is proportional to the photon flux within the detection area, can be calculated using

$$
I_{\pm l}(x_c, y_c, \delta) = B \iint_R dx\, dy |\psi_{\pm l}(x - x_c, y - y_c, \delta)|^2. \tag{3}
$$

The parameter B is a multiplier used to accommodate the values obtained from the calculations to match the experiment. The distribution of photons, which forms the self-image grating at $L_1 = L_T$, affects the count rate of photon detection, varying according to the effective open fraction $f_{\text{eff}} = \delta/d$. The numerical simulation based on the experiment setup shown in Fig. 2 utilized a wavelength of 785 nm, a Gaussian radius $w = 1.40$ mm, two grating periods $d = 200$ μm, a radius of $R = 25$ μm, and the center $(x_c, y_c) = (0, 0)$. The graph in Fig. 3 displays these numerical results, obtained from Eq. (3) for $l = 0$ at a distance of $L_2 = 3L_T$ (solid line).

The single-photon count rate can be employed to measure and distinguish the OAM l of the single photons by the Talbot effect. By positioning the detector using coordinates (x_c, y_c), the results yield notable variations in values for each l. For calculations, the first step involves normalizing the maximum value of the wave function for all l to be identical, using a scaling factor C_l. The second step entails determining the common coefficient B at a specific position (x_c, y_c) by normalizing the integrated intensity with an obtained experimental result at a particular value of l. For example, in this work, normalizing the value of B is based on the count rate data at the state $l = 1$ (see footnote a in Table I). With the Gaussian radius obtained from the previous experiment and $f_{\text{eff}} \simeq 0.20$, the estimated results closely match the experimental outcomes at the coordinate $(x_c, y_c) = (28.0, -68.5)$ μm as seen in Table I.

III. EXPERIMENTAL SETUP

Our single-photon vortex beam (Fig. 2) is produced by a 785-nm laser diode (model No. L785H1, Thorlabs), which is subsequently modulated with a linear polarizer (model No. LPVIS100-MP2, Thorlabs), and the polarization of the laser is rotated with a half waveplate (HWP) (model No. WPH10M-780, Thorlabs). This HWP in combination with the polarizing beam splitter (model No. PBS202, Thorlabs) can reduce the laser intensity to serve as the WCP source. A pulse signal of 1 MHz and 10 ns width from our home-made circuit [37] is used to drive the laser for this purpose. These pulses of single photons can be determined by the coincident signals of two avalanche photodiodes (APDs) (in single-photon counting modules F1 and F2). With these APDs
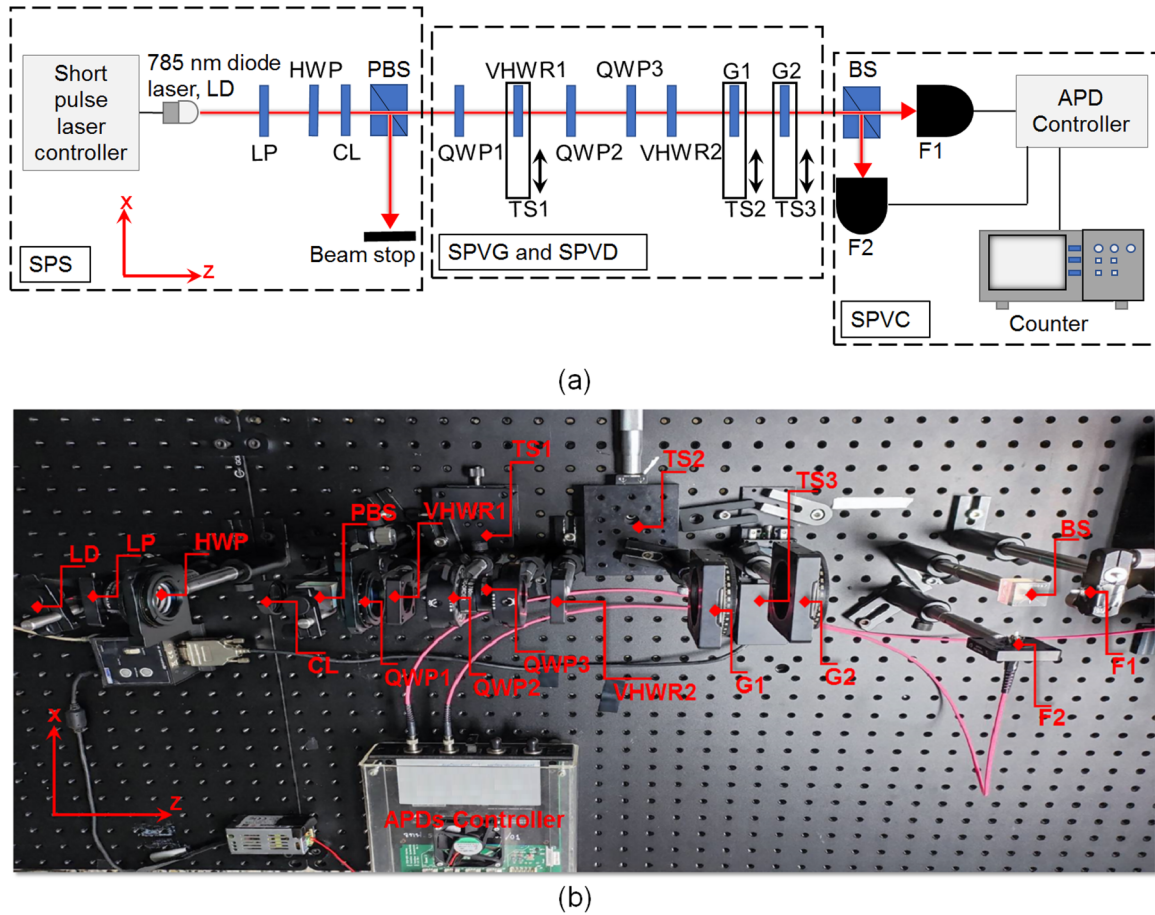
(a)

(b)

FIG. 2.   Single-photon vortex beam detection based on the Talbot effect with two-grating configuration: (a) schematic of the experiment and (b) actual setup. The single-photon source (SPS) was generated with the WCP method. The linear polarizer (LP) and the half waveplate (HWP) were used to regulate the polarization of the laser source (LD). The polarizing beam splitter (PBS) can select only the horizontal polarization to the next part of the setup. Therefore, the single-photon pulses or WCPs can be achieved with the polarization adjustment of the HWP. The single-photon vortex generator (SPVG) of the OAM states ($l = \pm1, \pm2$) was produced by the first vortex half-wave retarder (VHWR1) for $l = +1$ or -1 and by both VHWR1 and VHWR2 for $l = +2$ or -2. The two gratings G1 and G2 were set as the near-field Talbot configuration and mask grating, respectively. These two gratings were used for the single-photon vortex detection (SPVD) scheme [31,33]. The first APD (F1) was used as single-photon vortex counting (SPVC). The vortex beams of four sample OAM states ($l = \pm1, \pm2$) were sent one by one and the single-photon counting was used to identify these OAM states without using a single-photon camera. See the text for further details.

(F1 and F2) and a beam splitter (BS) (model No. BS014, Thorlabs), the single photon source can be checked with the coincidence measurement. The collimating lens (CL) (model No. LB1092-B-ML, Thorlabs) adjusts the laser beam to about 10 mm in diameter. The first VHWR (VHWR1) (model No. WPV10L-780, Thorlabs) transforms this Gaussian laser beam to a Laguerre-Gaussian beam of mode $l = +1$ or -1 in the single-photon vortex generator. A quarter waveplate (QWP1) (model No. WPQ10M-780, Thorlabs) produces the circular polarization in order to obtain the optical vortex beam from this VHWR1. Left- and right-handed circular polarizations provide OAM with the topological charge of $l = +1$ or -1, respectively. In order to extend to the OAM beam of $l = +2$ or -2, a second VHWR (VHWR2) (model No. WPV10L-780, Thorlabs) transforms the OAM beam of $l = +1$ or -1 to $l = +2$ or -2, respectively. The second and third QWPs (QWP2 and QWP3) (model No. WPQ10M-780, Thorlabs) are used to adjust the polarization of the laser to appropriate states of the VHWR2 [33]. The VHWR1 can move in to accompany the VHWR2 to obtain $l = \pm2$ or move out to get $l = \pm1$ from the VHWR2 by using a translation stage (TS1) (model No. GCM-122101M, Daheng). The Talbot effect with two-grating configuration is recommended for the single-photon vortex detection where the first grating ($d = 200$ μm, chromium on glass, Edmund Optics Inc.) is a diffraction grating and the second grating acts as a mask. The spacing between the two gratings is set at one Talbot length, while the distance between the second grating and the fiber optics F1 and F2 (FC/FC MM.Patch cord 1 m, OM4, 50/125) is three Talbot lengths. The grating G1 can be moved transversely with the translation stage TS2 (model No. PT1/M, Thorlabs) to check the overlap between the two gratings. This grating overlap can also be used to optimize the resolution of vortex identification. The mask grating G2 can also be moved transversely with the stage TS3 (model No. MTS25/M-Z8, Thorlabs) to check the Talbot pattern. In our recent study, the position of the optical fiber F1 (the circle with radius of R in Fig. 1) was optimized to find the best condition for the measurements.
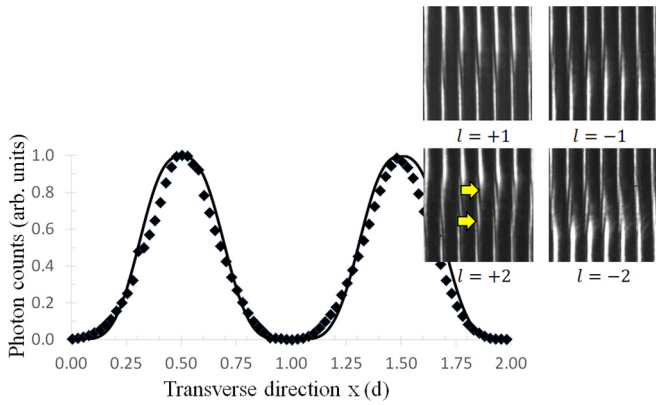
FIG. 3. Interference pattern of a single-photon vortex beam. The spacing between the two gratings (G1 and G2) was set at one Talbot length and the distance between G2 and the fiber optics (F1 and F2) of the APDs was three Talbot lengths. The G2 was transversely scanned in steps of 5 μm. The x axis represents the grating periods d. The insets show the experimental results of the Talbot interference patterns imprinted with the optical vortex recorded by a CCD camera to verify the OAM states before switching to the single-photon vortex experiments. Numbers and directions of the tilted dark stripes in the middle of the interference fringes identify the order and charge of the vortex beam, respectively. For example, the two arrows point to the beam of $l = +2$ in this case.

IV. RESULTS

Figure 3 represents results of the single-photon Talbot pattern scanning with the mask grating G2 to check the alignment first. The result, taken at one Talbot length behind the first grating G1, shows a fine self-image with high signal-to-noise ratio of 27 and high visibility of above 90%. The insets in Fig. 3 are the Talbot interference patterns with vortex beams of $l = \pm 1, \pm 2$ indicated by the tilted dark stripes in the middle of the interference fringes [27,28,33]. These interference patterns were recorded by a CCD camera to verify the OAM states before switching to the single-photon vortex experiments. Our main objective is to resolve different OAM states without using a single-photon camera. To do this, the mask grating G2 takes a role in this task. The photon-count modulation accompanying the two gratings G1 and

TABLE I. Single-photon counts from APD1 (F1) with different OAM states l.

OAMs l	Theoretical simulations (kHz)	Experimental results (kHz)
−1	3.59	3.61
+1	3.02[a]	3.02
−2	3.29	3.25
+2	2.22	2.20

[a]Normalization of B based on the count rate data at the state $l = 1$.

G2 can significantly distinguish these single-photon vortex beams with different photon counts. The photon counts of $l = \pm 1, \pm 2$ in both simulations and experiments are exhibited in Table I. The calculations are normalized with the parameter B to compare the simulations with the experimental results; they are closely matched. Without using a single-photon camera and image processing, our scheme can provide a robust and fast technique for single-photon vortex detection.

V. CONCLUSIONS

In conclusion, we proposed a different approach to single-photon vortex beam detection and identification. The method is based on the Talbot effect in cooperation with the use of a mask grating. The OAM beams with $l = \pm 1$ and ± 2 were used to demonstrate the concept. These four vortex states give significantly different photon counts. We are convinced that our method can be useful in the fields of quantum information and even quantum metrology using a single-photon vortex source.

[1] L. Allen, M. W. Beijersbergen, R. J. C. Spreeuw, and J. P. Woerdman, Phys. Rev. A **45**, 8185 (1992).

[2] A. M. Yao and M. J. Padgett, Adv. Opt. Photon. **3**, 161 (2011).

[3] S. W. Hancock, S. Zahedpour, A. Goffin, and H. M. Milchberg, Optica **6**, 1547 (2019).

[4] J. Wang, Q. Wang, J. Liu, and D. Lyu, AVS Quantum Sci. **4**, 031701 (2022).

[5] A. Vaziri, G. Weihs, and A. Zeilinger, Phys. Rev. Lett. **89**, 240401 (2002).

[6] A. Manzalini, Quantum Rep. **2**, 579 (2020).

[7] M. Erhard, R. Fickler, M. Krenn, and A. Zeilinger, Light: Sci. Appl. **7**, 17146 (2018).

[8] N. J. Cerf, M. Bourennane, A. Karlsson, and N. Gisin, Phys. Rev. Lett. **88**, 127902 (2002).

[9] J. C. García-Escartín and P. Chamorro-Posada, J. Opt. **13**, 064022 (2011).

[10] A. Mair, A. Vaziri, G. Weihs, and A. Zeilinger, Nature (London) **412**, 313 (2001).

[11] J. Romero, D. Giovannini, S. Franke-Arnold, S. M. Barnett, and M. J. Padgett, Phys. Rev. A **86**, 012334 (2012).

[12] B. C. Hiesmayr, M. J. A. de Dood, and W. Löffler, Phys. Rev. Lett. **116**, 073601 (2016).

[13] M. Malik, M. Erhard, M. Huber, M. Krenn, R. Fickler, and A. Zeilinger, Nat. Photon. **10**, 248 (2016).

[14] W. Wang, K. Zhang, and J. Jing, Phys. Rev. Lett. **125**, 140501 (2020).

[15] T. Stav, E. Maguid, D. Oren, V. Kleiner, E. Hasman, and M. Segev, Science **361**, 1101 (2018).

[16] X. L. Wang, X. D. Cai, Z. E. Su, M. C. Chen, D. Wu, L. Li, N. L. Liu, C. Y. Lu, and J. W. Pan, Nature (London) **518**, 516 (2015).

[17] M. Mirhosseini, O. S. Magaña-Loaiza, M. N. O'Sullivan, B. Rodenburg, M. Malik, M. P. J. Lavery, M. J. Padgett, D. J. Gauthier, and R. W. Boyd, New J. Phys. **17**, 033033 (2015).

[18] Z. Wang, R. Malaney, and B. Burnett, Phys. Rev. Appl. **14**, 064031 (2020).

[19] Q. K. Wang, F.-X. Wang, J. Liu, W. Chen, Z.-F. Han, A. Forbes, and J. Wang, Phys. Rev. Appl. **15**, 064034 (2021).

[20] J. Leach, M. J. Padgett, S. M. Barnett, S. Franke-Arnold, and J. Courtial, Phys. Rev. Lett. **88**, 257901 (2002).

[21] G. C. G. Berkhout, M. P. J. Lavery, J. Courtial, M. W. Beijersbergen, and M. J. Padgett, Phys. Rev. Lett. **105**, 153601 (2010).

[22] M. P. J. Lavery, D. J. Robertson, G. C. G. Berkhout, G. D. Love, M. J. Padgett, and J. Courtial, Opt. Express **20**, 2110 (2012).

[23] S. J. Tempone-Wiltshire, S. P. Johnstone, and K. Helmerson, Sci. Rep. **6**, 24463 (2016).

[24] W. Zhang, J. Wang, F. Li, L. Chen, and E. Karimi, Laser Photon. Rev. **11**, 1600163 (2017).

[25] H. F. Talbot, Philos. Mag. Ser. **9**, 401 (1836).

[26] S. Deachapunya, S. Srisuphaphon, P. Panthong, T. Photia, K. Boonkham, and S. Chiangga, Opt. Express **24**, 20029 (2016).

[27] P. Panthong, S. Srisuphaphon, A. Pattanaporkratana, S. Chiangga, and S. Deachapunya, J. Opt. **18**, 035602 (2016).

[28] P. Panthong, S. Srisuphaphon, S. Chiangga, and S. Deachapunya, Appl. Opt. **57**, 1657 (2018).

[29] D. A. Ikonnikov, S. A. Myslivets, M. N. Volochaev, V. G. Arkhipkin, and A. M. Vyunishev, Sci. Rep. **10**, 20315 (2020).

[30] S. Srisuphaphon, S. Buathong, and S. Deachapunya, J. Opt. Soc. Am. B **37**, 2021 (2020).

[31] S. Buathong, S. Srisuphaphon, and S. Deachapunya, J. Opt. **24**, 025602 (2022).

[32] S. Srisuphaphon, S. Buathong, and S. Deachapunya, Opt. Laser Technol. **148**, 107746 (2022).

[33] S. Deachapunya, S. Srisuphaphon, and S. Buathong, Sci. Rep. **12**, 6061 (2022).

[34] C. You, A. C. Nellikka, I. D. Leon, and O. S. Magaña-Loaiza, Nanophotonics **9**, 1243 (2020).

[35] F. Mostafavi, Z. Jafari, M. L. J. Lollie, C. You, I. D. Leon, and O. S. Magaña-Loaiza, Nanophotonics **11**, 3299 (2022).

[36] W. B. Case, M. Tomandl, S. Deachapunya, and M. Arndt, Opt. Express **17**, 20966 (2009).

[37] S. Buathong, J. Janpoon, N. Suksawat, and S. Deachapunya, J. Phys.: Conf. Ser. **2145**, 012058 (2021).